Second-Harmonic Generation by Damped Alfvén Waves and Helicons in Pure and Doped Bismuth

R. T. BATE AND W. R. WISSEMAN
Texas Instruments Incorporated, Dallas, Texas 75222
(Received 30 December 1968)

The results of a study of second-harmonic generation by damped Alfvén waves and helicons propagating parallel to the static magnetic field along the three principal axes of pure and tellurium-doped bismuth are reported. The observed anisotropy and polarization dependences are shown to be consistent with the occurrence of a magnetic dipole nonlinearity caused by the influence of the magnetic field of the wave on the conductivity of the medium. A theory of harmonic generation by plane waves propagating in a semi-infinite anisotropic conducting medium and in a slab is developed and applied to this case. It is shown that the concept of magnetic point groups can be applied to the determination of the form of the third-rank tensors governing the effect, which leads to the conclusion that the forms of these tensors are, in fact, known for all crystal classes. A method of calculating these tensors after their reduction by symmetry from standard transport theory for bismuth is developed and results for some of the coefficients relevant to the experiments are given.

I. INTRODUCTION

THE generation of second-harmonic signals by damped Alfvén waves and helicons propagating in bismuth parallel to the static magnetic field has been reported briefly in an earlier paper.[1] We present here a fuller account of these experiments along with a more precise mathematical treatment of the problem.

The primary source of the harmonic is believed to be a nonlinearity of the magnetic-dipole type[2] produced by the dependence of the resistivity tensor (or the inverse dielectric tensor)[3] on the rf magnetic field component of the wave. This conclusion is supported by the observed dependence of the polarization of the harmonic signal on the polarization of the fundamental in the case of damped Alfvén wave propagation which was reported earlier.[1] Nonlinearity due to the dependence of the resistivity on the electric field should be negligible in this case, since the electric field in the sample does not exceed 1 V/cm. Hot-electron effects, which can cause harmonic generation in semiconductors,[4] should be negligible in semimetals and, if present, would be expected to produce primarily third-harmonic signals. Because of the large, field-dependent diamagnetic susceptibility of Bi, nonlinearities due to the dependence of the magnetic permeability on the rf magnetic field may have some influence. However, our estimates indicate that this contribution is negligible compared to the one under consideration.

The simplest nonlinearity of the general type we are considering would be found in a semimetal containing equal concentrations of electrons and holes in identical spherical bands. In this case, a "fast" Alfvén mode[5] will propagate with its wave vector $\mathbf{k}$ perpendicular to the static magnetic field $\mathbf{B}_0$. The rf magnetic field $\mathbf{b}$ of this mode is parallel to $\mathbf{B}_0$, so that the total magnetic field in the direction of $\mathbf{B}_0$ is B_0+b. Since, for $\omega_c\tau\gg1$, the velocity V_a of this mode is just $B/(2\mu_0 nm^*)^{1/2}$, the wave "modulates" its own velocity with $\delta V_a/V_a=b/B_0$, generating a second harmonic. The notation is that of Ref. 5.

If, in the preceding example, the static field $\mathbf{B}_0$ is rotated through 90° so that it is parallel to $\mathbf{k}$, no second harmonic will be observed. This result is predicted by a detailed solution of the problem, but is also a result of general symmetry restrictions which require that no second harmonic be generated when both $\mathbf{B}_0$ and $\mathbf{k}$ are perpendicular to a reflection plane of the crystal (or of the Fermi surface). A proof of this will be found in Appendix B. In a cubic crystal, for example, this restriction rules out the observation of second harmonics for $\mathbf{B}_0$ and $\mathbf{k}$ along the [100] or [110] axes, but not along [111]. In bismuth (point group $\bar{3}m$), the effect is allowed for $\mathbf{B}_0$ and $\mathbf{k}$ along bisectrix and trigonal axes, but not along the binary axis.

The paper is organized as follows: In Sec. II we develop a theory of harmonic generation in anisotropically conducting media treating the case of normal incidence on a semi-infinite medium. The formulation of the wave equation in terms of the resistivity tensor, which is real and independent of frequency for $\omega\tau\ll1$, is employed. The development parallels that of Bloembergen and Pershan[6] for isotropic nonconducting media. The case of normal incidence on a slab is treated in Appendix A. Symmetry restrictions on nonlinear coefficients are found by application of magnetic point groups in Appendix B, and a method for calculating these coefficients from the Fermi-surface model is outlined in Appendix C.

Section III covers the experimental procedure, and Sec. IV includes a detailed discussion of the results for damped Alfvén waves propagating along each of the

[1] W. R. Wisseman and R. T. Bate, Phys. Rev. Letters **20**, 1492 (1968); **21**, 330 (1968).
[2] P. S. Pershan, Phys. Rev. **130**, 919 (1963).
[3] L. D. Landau and E. M. Lifshitz, *Electrodynamics of Continuous Media* (Pergamon Press, Inc., Oxford, 1960), p. 331.
[4] J. Maurer, A. Libchaber, and J. Bok, in *Proceedings of the Symposium on Plasma Effects in Solids, Paris, 1964* (Dunod Cie., Paris, 1965), pp. 49–52.
[5] S. J. Buchsbaum, in *Proceedings of the Symposium on Plasma Effects in Solids, Paris, 1964* (Dunod Cie., Paris, 1965), pp. 3–18.
[6] N. Bloembergen and P. S. Pershan, Phys. Rev. **128**, 606 (1962).

principal axes of pure Bi, and some results for helicons in Te-doped Bi. Some final conclusions are drawn in Sec. V.

II. THEORY

Penz[7] has determined the wave equation from Maxwell's equations for a general magnetoresistivity tensor $\boldsymbol{\varrho}(\mathbf{B})$ relating the electric field to the current density for the case where the displacement current is neglected. The equation can be written as (in mks units with $\mu=\mu_0$)

$$\nabla\times(\boldsymbol{\varrho}\nabla\times\mathbf{b})=-\mu_0(\partial\mathbf{b}/\partial t). \tag{1}$$

Equation (1) has plane wave solutions of the form

$$\mathbf{b}(\omega,k)=\mathbf{b}^0e^{i(\omega t-kz)}$$

for a wave propagating in the z direction and $\mathbf{b}^0$ in the xy plane when the dependence of $\boldsymbol{\varrho}$ on $\mathbf{b}$ is neglected. The effect of $\mathbf{b}$ can be included if we write

$$\boldsymbol{\varrho}(\mathbf{B})=\boldsymbol{\varrho}(\mathbf{B}_0+\mathbf{b})=\boldsymbol{\varrho}(\mathbf{B}_0)+\delta\boldsymbol{\varrho}(\mathbf{B}_0,\mathbf{b}), \tag{2}$$

where $\mathbf{B}_0$ is the constant applied magnetic field. We are interested in the solution of Eq. (1) of the form $\mathbf{b}=\mathbf{b}_f(\omega)+\mathbf{b}_h(2\omega)$. If the harmonic signal is small relative to the fundamental, then $\delta\boldsymbol{\varrho}(\mathbf{B}_0,\mathbf{b})\approx\delta\boldsymbol{\varrho}(\mathbf{B}_0,\mathbf{b}_f)$. This expression can then be expanded to give

$$\delta\boldsymbol{\varrho}(\mathbf{B}_0,\mathbf{b}_f)=\delta\boldsymbol{\varrho}(\mathbf{B}_0,\mathbf{b}_f{}^0)e^{i(\omega t-kz)}$$

to first order in $\mathbf{b}_f$. If we use this expression for $\delta\boldsymbol{\varrho}$ and substitute Eq. (2) in Eq. (1), we obtain an equation for $\mathbf{b}_f$ and $\mathbf{b}_h$ which can be separated as follows:

$$\nabla\times(\boldsymbol{\varrho}_0\nabla\times\mathbf{b}_f)+\mu_0(\partial\mathbf{b}_f/\partial t)=0 \tag{3}$$

and

$$\nabla\times(\boldsymbol{\varrho}_0\nabla\times\mathbf{b}_h)+\mu_0(\partial\mathbf{b}_h/\partial t)=-\nabla\times(\delta\boldsymbol{\varrho}\nabla\times\mathbf{b}_f), \tag{4}$$

where Eq. (3) holds at ω and Eq. (4) at 2ω and $\boldsymbol{\varrho}_0\equiv\boldsymbol{\varrho}(\mathbf{B}_0)$. We are not considering contributions to these equations from solutions at higher harmonic frequencies, and we are also neglecting the term $\nabla\times(\delta\boldsymbol{\varrho}\nabla\times\mathbf{b}_h)$ which contributes to Eq. (3) since we take the nonlinear effect to be small. We also assume $\boldsymbol{\varrho}_0$ to be independent of frequency. This is true *only* when $\omega\tau\ll1$. In bismuth, the asymptotic dependences of the relevant components of $\boldsymbol{\varrho}$ on B_0 and on the relaxation time τ for large B_0 are

$$\rho_{xx},\rho_{yy}\propto\tau^{-1},$$
$$\rho_{xy},\rho_{yx}\propto B_0,$$

when $n\neq p$ (helicon propagation) and

$$\rho_{xx},\rho_{yy}\propto B_0{}^2\tau,$$
$$\rho_{xy},\rho_{yx}\propto B_0,$$

when $n=p$ (damped Alfvén wave propagation).

Penz has solved Eq. (3) and obtained the dispersion relation for the fundamental wave and the ratio of the field components for helicon propagation:

$$k_\pm{}^2=\frac{\mu_0\omega}{2}\left(\frac{\pm[-4\rho_{xy}\rho_{yx}-(\rho_{xx}-\rho_{yy})^2]^{1/2}-i(\rho_{xx}+\rho_{yy})}{\rho_{xx}\rho_{yy}-\rho_{xy}\rho_{yx}}\right), \tag{5}$$

$$f_\pm=\frac{b_{fx}{}^0}{b_{fy}{}^0}=\frac{2\rho_{yx}}{(\rho_{yy}-\rho_{xx})\pm i[-4\rho_{xy}\rho_{yx}-(\rho_{xx}-\rho_{yy})^2]^{1/2}}, \tag{6}$$

where $\rho_{xy}\neq0$, $\rho_{yx}\equiv\rho_{yx}(\mathbf{B}_0)$, etc. Two elliptically polarized modes (labeled + and −) are possible in this case. When $\rho_{xy}=0$, we have the simpler relation

$$k_x=(1-i)(\mu_0\omega/2\rho_{yy})^{1/2}, \tag{7}$$

where the subscript x on k indicates linear polarization in the x direction. Equation (7) applies to Alfvén wave propagation.

We treat the term on the right side of Eq. (4) as the source of the harmonic following Bloembergen and Pershan.[6] The solution of Eq. (4) is

$$b_{hx}=b_{sx}+b_{px}=b_{sx}{}^0e^{i(2\omega t-k_sz)}+b_{px}{}^0e^{i(2\omega t-2kz)} \tag{8}$$

for the x component. The term b_{sx} is a solution of the homogeneous equation which results from setting the source term in Eq. (4) equal to zero, and b_{px} is a particular solution with the source term included. The wave vector k_s is related to 2ω by Eq. (5) or (7). Subscripts on k_s and k indicating polarization have been omitted. The appropriate subscript for k_s depends on whether Eq. (5) or (7) applies (helicons or Alfvén waves) and on whether we want b_{hx} or b_{hy}. The subscript on k depends on the polarization of the fundamental.

The coefficient $b_{px}{}^0$ and similarly $b_{py}{}^0$ can be evaluated from Eq. (4) in terms of $b_{fx}{}^0$ and $b_{fy}{}^0$ and the components of the resistivity tensor. We get

$$\begin{aligned}b_{pi}{}^0=\{&[-(2\rho_{ii}+i\omega\mu_0/k^2)\delta\rho_{jj}{}^0+2\rho_{ji}\delta\rho_{ij}{}^0]b_{fi}{}^0\\&+[(2\rho_{ii}+i\omega\mu_0/k^2)\delta\rho_{ji}{}^0-2\rho_{ji}\delta\rho_{ii}{}^0]b_{fj}{}^0\}\\&\times\{(2\rho_{ii}+i\omega\mu_0/k^2)(2\rho_{jj}+i\omega\mu_0/k^2)-4\rho_{ij}\rho_{ji}\}^{-1},\end{aligned} \tag{9}$$

where $i=x$ or y and $j=y$ or x. This equation can be simplified considerably when the orientations of $\mathbf{B}_0$ and $\mathbf{b}_f$ relative to the principal axes of the crystal are specified and the expressions for the components of $\delta\boldsymbol{\varrho}^0$ are determined. In Appendix B it is shown that these expressions have the general form

$$\delta\rho_{ij}{}^0=[S_{ijk}(\mathbf{B}_0)+A_{ijk}(\mathbf{B}_0)]b_k{}^0, \tag{10}$$

where the nonlinear coefficients $S_{ijk}(\mathbf{B}_0)$ and $A_{ijk}(\mathbf{B}_0)$ are components of third-rank tensors which depend on the static field $\mathbf{B}_0$. When $\mathbf{B}_0=0$, the $S_{ijk}(\mathbf{B}_0)$ vanish and the A_{ijk} become the usual weak-field Hall tensor coefficients.

If $\mathbf{B}_0$ and $\mathbf{k}$ are perpendicular to a plane in which the crystal or the Fermi surface possesses reflection symmetry, it is also shown in Appendix B that the nonlinear coefficients which can contribute to $b_{pi}{}^0$ via Eqs. (9) and (10) vanish. Since, as we shall see, the

[7] P. A. Penz, J. Appl. Phys. **38**, 4047 (1967); **39**, 1922 (1968).

TABLE I. Expression for b_{pi}^0 [Eq. (9)] and k_{si} [Eq. (7)] for damped Alfvén-wave propagation.

Magnetic-field orientations and k_i	b_{pi}^0 and k_{si}	
$\mathbf{B}_0 \| 1$[a]	$b_{p2}^0 = b_{p3}^0 = 0$	
$\mathbf{B}_0 \| 2$[b]		
$\mathbf{b}_f \| 1$	$b_{p1}^0 = \dfrac{-2\rho_{13}S_{311}b_{f1}^{0\,2}}{\rho_{33}(2\rho_{11}-\rho_{33})}$	$k_{s1} = \sqrt{2}k_1$
$k_1 = (1-i)\left(\dfrac{\mu_0\omega}{2\rho_{33}}\right)^{1/2}$	$b_{p3}^0 = \dfrac{-S_{311}b_{f1}^{0\,2}}{2\rho_{11}-\rho_{33}}$	$k_{s3} = \left(\dfrac{2\rho_{33}}{\rho_{11}}\right)^{1/2} k_1$
$\mathbf{b}_f \| 3$	$b_{p1}^0 = \dfrac{(\rho_{11}A_{313}+\rho_{13}S_{113})b_{f3}^{0\,2}}{\rho_{11}(2\rho_{33}-\rho_{11})}$	$k_{s1} = \left(\dfrac{2\rho_{11}}{\rho_{33}}\right)^{1/2} k_3$
$k_3 = (1-i)\left(\dfrac{\mu_0\omega}{2\rho_{11}}\right)^{1/2}$	$b_{p3}^0 = \dfrac{[-S_{113}(2\rho_{33}-\rho_{11})+2\rho_{13}A_{313}]b_{f3}^0}{\rho_{11}(2\rho_{33}-\rho_{11})}$	$k_{s3} = \sqrt{2}k_3$[2]
$\mathbf{B}_0 \| 3$[c]		
$k = (1-i)\left(\dfrac{\mu_0\omega}{2\rho_{11}}\right)^{1/2}$	$b_{p1}^0 = \dfrac{-2S_{222}b_{f1}^0 b_{f2}^0}{\rho_{11}}$	$k_s = \sqrt{2}k$
	$b_{p2}^0 = \dfrac{-S_{222}(b_{f1}^{0\,2}-b_{f2}^{0\,2})}{\rho_{11}}$	

[a] All components of $\delta\mathbf{Q}^0$ are zero.
[b] The results are very complicated for polarizations along arbitrary axes.
[c] $\rho_{11}=\rho_{22}$ and $\rho_{12}=\rho_{21}=0$.

second-harmonic signal is proportional to b_{pi}^0, this means that no second harmonic will be generated when the fundamental wave propagates parallel to $\mathbf{B}_0$ and perpendicular to a reflection plane.

From the foregoing considerations, the feature of the Fermi surface which is responsible for the observed harmonic immediately becomes apparent. If the ellipsoidal electron portions of the Fermi surface were not tilted out of the trigonal plane, then all three principal crystallographic planes would be reflection planes, and no second harmonics would appear for $\mathbf{B}_0$ and $\mathbf{k}$ along a principal axis. This conclusion is confirmed by the calculation of certain nonlinear coefficients in terms of Fermi-surface parameters in Appendix C, where they are found to be proportional to m_4, the off-diagonal electron mass tensor component, which is nonzero only by virtue of the tilt of the ellipsoids [see Eqs. (C6) and (C7)]. It is therefore the tilting of the electron ellipsoids out of the trigonal plane which is responsible for the effect when $\mathbf{B}_0$ and $\mathbf{k}$ are along a principal axis.

The coefficients b_{sx}^0 can be evaluated in terms of b_{px}^0 by applying the appropriate boundary conditions. If $\mathbf{b}_f$ is a plane wave normally incident upon a semi-infinite medium ($\mu=\mu_0$) and we require $\mathbf{b}_h$ and $\mathbf{E}_h$ to be continuous across the boundary, Eq. (8) becomes

$$b_{hx} = -\left(\frac{1+\omega/kc}{1+2\omega/k_sc}\right)b_{px}^0 e^{i(2\omega t-k_sz)} + b_{px}^0 e^{i(2\omega t-2kz)}. \quad (11)$$

In Appendix A we consider the case of harmonic generation by a plane wave at normal incidence upon a slab. We have assumed finite damping in this case because it leads to considerable simplification of the results. The source term which was used in Eq. (4) was determined by applying the above boundary conditions to the fundamental wave. The transmitted fundamental ($|kc/\omega| \gg 1$) is given by

$$\mathbf{b}_{ftx} = \frac{-2i\omega\mathbf{b}_f^0}{kc\sin kl} e^{i\omega(t-l/c)}. \quad (12)$$

Application of the same boundary conditions to the harmonic wave and the approximation $|k_sc/2\omega| \gg 1$ gives

$$b_{htx} = \frac{8i\omega b_{px}^0 \sin[\frac{1}{2}(2k+k_s)l]\sin[\frac{1}{2}(2k-k_s)l]e^{i2\omega(t-l/c)}}{k_sc\sin k_sl\sin^2 kl} \quad (13)$$

for the transmitted harmonic signal. The subscripts denoting polarization are omitted from k and k_s, and b_{px}^0 is defined by Eq. (9). In Eq. (13), and also in Eq. (11), k and b_{px}^0 depend on the polarization of the fundamental and k_s depends on the desired component of the harmonic signal. For convenience of notation, we have written Eq. (13) in component form and omitted the subscripts from k and k_s denoting polarization.

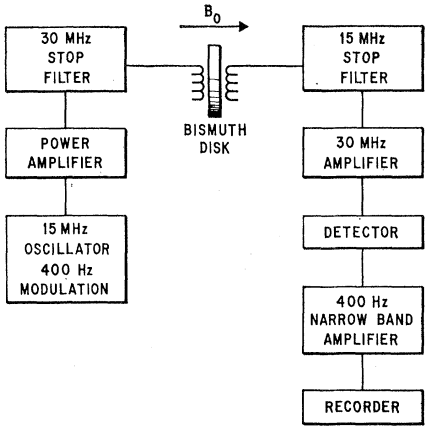

FIG. 1. Experimental arrangement for observing harmonic generation.

We have tabulated the appropriate expressions for b_{pi}^0 [Eq. (9)] and the corresponding k and k_s [Eqs. (5) and (7)] for damped Alfvén wave propagation along principal axes in Table I and helicon propagation along principal axes in Table II. The results are expressed in terms of the appropriate nonlinear coefficients determined in Appendix B. The harmonic signal can then be determined using Eq. (13). (We have used the usual notation for the principal axes of Bi, i.e., 1-binary, 2-bisectrix, 3-trigonal.)

We see from Tables I and II that for both damped Alfvén wave and helicon propagation, the source of the harmonic b_{pi}^0 vanishes for $\mathbf{B}_0\|1$ due to the fact that the binary plane is a reflection plane. Of the other two principal orientations of $\mathbf{B}_0$, the results for $\mathbf{b}_0\|3$ are far simpler owing to the trigonal symmetry. The harmonic signal generated by a damped Alfvén signal of arbitrary linear polarization is given for this case in Table I. For helicon propagation along the trigonal direction, it should be noted that the harmonic generated by the nonpropagating circular polarization has the same magnitude as that generated by the propagating helicon. For the complicated bisectrix case, the results for damped Alfvén wave propagation could only be expressed conveniently for the fundamental wave polarized in a principal direction. This is true because there are four pertinent nonlinear coefficients which appear in Table VII. (One of these coefficients, S_{333}, does not contribute for the cases considered in Table I.) We have not calculated the harmonic signal for helicon propagation in the bisectrix direction. Further comments about the results presented in these tables are made in Sec. IV.

TABLE II. Expressions for b_{pi}^0 [Eq. (9)] and $k_{s\pm}$ [Eq. (5)] for helicon propagation.

Magnetic-field[a] orientations and $k_\pm$	b_p^0 and $k_{s\pm}$[b]
$\mathbf{B}_0\|3$	
$b_f^0(\hat{1}-i\hat{2})$	
$k_+\approx\left(\frac{\mu_0\omega}{\rho_{12}}\right)^{1/2}\left(1-\frac{i\rho_{11}}{2\rho_{12}}\right)$	$\frac{2S_{222}b_f^{02}(\hat{1}+i\hat{2})}{3\rho_{12}}$
$b_f^0(\hat{1}+i\hat{2})$	
$k_-\approx\left(\frac{\mu_0\omega}{\rho_{12}}\right)^{1/2}\left(\frac{\rho_{11}}{2\rho_{12}}-i\right)$	$\frac{2S_{222}b_f^{02}(\hat{1}-i\hat{2})}{3\rho_{12}}$

[a] No effect predicted when $\mathbf{B}_0\|1$. Results are very complicated when $\mathbf{B}_0\|2$.
[b] Only $k_s=k_{s+}=\sqrt{2}k_+$ is important since the harmonic is severely attenuated when $k_s=k_{s-}=\sqrt{2}k_-$.

III. EXPERIMENTAL PROCEDURE

The important features of the experimental arrangement are shown for harmonic generation in Fig. 1. A similar arrangement was used to observe mixing. The filters were required to eliminate spurious 30-MHz signals which were present in the input signal or generated by the large fundamental signal in the detector. Since a sensitive amplifier with a fairly narrow bandwidth was required to detect the harmonic signal generated in the sample, it was inconvenient to make measurements as a function of frequency. For all of the harmonic-generation measurements reported here, the input frequency was 15.0 MHz. Mixing of input frequencies of 12.5 and 17.5 MHz was also observed so that the detected signal in both cases was 30 MHz. A transmission curve was measured as a function of magnetic field for the fundamental signal with the detector coil connected directly to a Hewlett-Packard Model 8405 vector voltmeter which also measured the relative phase of the signal. The harmonic signal was then measured with the system shown in Fig. 1 which was calibrated using the vector voltmeter.

The samples were cut from single crystals grown by the Czochralski method using 99.9999% pure bismuth. The melt was doped with tellurium to obtain the samples used for helicon propagation. Slices from each ingot were cleaved to determine the approximate direction of the trigonal axis, and the ingots were then oriented by back-reflection Laue photographs to an accuracy of $\pm1°$. The samples were in the form of disks typically 12 mm in diam by 1 or 2 mm thick. Back-reflection Laue photographs were also made for the disks as a check on the orientation of the principal axes. The samples were soldered with a low-melting-point solder into a copper holder so that the leakage signal around the sample could be eliminated.

Ten-turn rectangular coils with $\sim$1-mm^2 cross section were used in both the drive and the detector circuits. The drive and detector coils were aligned with their axes either parallel or perpendicular to each other and in principal directions. It is estimated that the coils were aligned parallel to principal axes in the plane perpendicular to $\mathbf{k}$ to within $\pm3°$.

IV. RESULTS AND DISCUSSION

In this section the experimental results which we have obtained for harmonic generation by damped Alfvén waves and helicons are presented along with a comparison of these results with the theory described in Sec. II for some of the simplest cases. Essentially, the same results were obtained when two signals were mixed in the sample and the sum frequency was observed. Some of these data were presented in an earlier paper[1] along with a simplified theoretical model. This model successfully described the polarization of the harmonic generated by a damped Alfvén wave when $\mathbf{B}_0$, $\mathbf{k}\|3$ and the lack of a harmonic signal when $\mathbf{B}_0$, $\mathbf{k}\|1$. We were not, however, able to account satisfactorily for the polarization of the harmonic generated by damped Alfvén waves when $\mathbf{B}_0$, $\mathbf{k}\|2$. Another limitation of the approach used in our earlier paper was the neglect of the phase relationships between harmonic signals generated at different points in the nonlinear material. Such phase relationships are taken into account by the theory developed in Sec. II. No attempt has been made to treat theoretically the large quantum oscillations which are observed for some orientations. This would require a detailed theory of the Shubnikov–de Haas effect in bismuth. However, the periods of these oscillations are in good agreement with recent de Haas–Van Alphen data.[8]

A. Damped Alfvén

All of the damped Alfvén measurements were made with $\mathbf{B}_0\|\mathbf{k}\|$(principal axis) and the axes of the drive and pickup coils along principal axes and perpendicular to $\mathbf{k}$. The harmonic signal was found to depend on the square of the fundamental signal as is shown in Fig. 2. This result is in agreement with the expressions obtained in Sec. II. In almost all cases where a harmonic signal was observed, there was a maximum in the signal at low magnetic fields (1–3 kG) as is shown in Fig. 3. If the expression for the harmonic signal given in Ref. 1 or Eq. (11) of this paper is used, a maximum in the harmonic is predicted as was mentioned in Ref. 1. Our use of those expressions was incorrect, however, since in addition to the difficulties already pointed out, they apply only to an infinite medium. If the expression for harmonic generation in a slab given by Eq. (13) is used, no maximum is predicted. This is a result of the fact that the dielectric mismatch between the slab and air depends on B_0. We now believe that the maximum in the harmonic curve is a geometric effect due to the fact that the size of the drive and pickup coils is comparable to the slab thickness. This conjecture is supported by the fact that the damped Alfvén transmission curve saturates for large B_0 as is shown in Fig. 3. This should not occur according to Eq. (12) for transmission through a slab. Bartelink and Nordland[9] observed similar effects in their damped Alfvén wave studies and found by using coils of different sizes that the saturation is a geometric effect. In our experiment it would be difficult to make the coil size small compared with the slab thickness to eliminate this geometric effect due to the low level of the harmonic signal. In principle, a geometric correction factor could be calculated from the damped Alfvén transmission if the correct value of τ is known. Comparison of the harmonic curve with theory could then be made using Eq. (13)

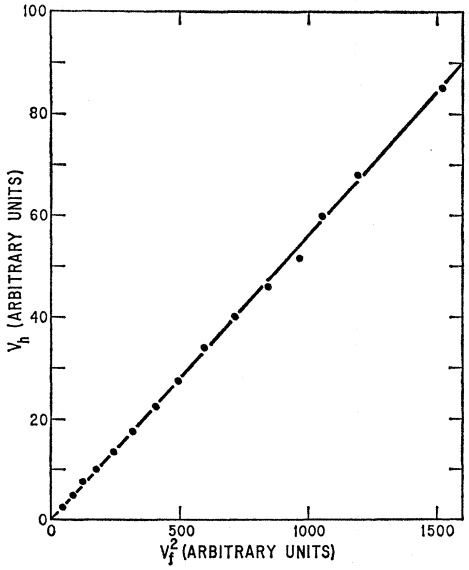

FIG. 2. Amplitude of 30-MHz harmonic signal voltage (1 component) as a function of the square of the 15-MHz fundamental damped Alfvén signal voltage (polarized ||1) for bismuth sample 77-4. The data were taken at 4.2°K with a magnetic field of 1.5 kG with $\mathbf{B}_0,\mathbf{k}\|2$.

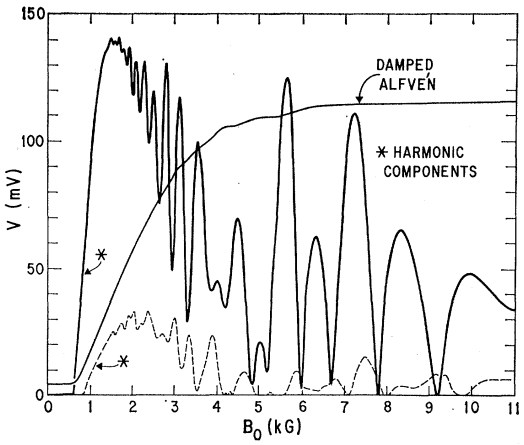

FIG. 3. Amplitude (times 3×10^4) of 30-MHz harmonics generated by 15-MHz damped Alfvén wave (also shown) as a function of magnetic field at 4.2°K for bismuth sample 77-4, with $\mathbf{B}_0,\mathbf{k}\|2$ and the fundamental damped Alfvén wave polarized ||1. The magnitude of b_{h11} is given by the solid curve and the magnitude of b_{h13} is given by the dashed curve.

[8] R. N. Bhargava, Phys. Rev. **156**, 785 (1967).

[9] D. J. Bartelink and W. A. Nordland, Phys. Rev. **152**, 556 (1966).

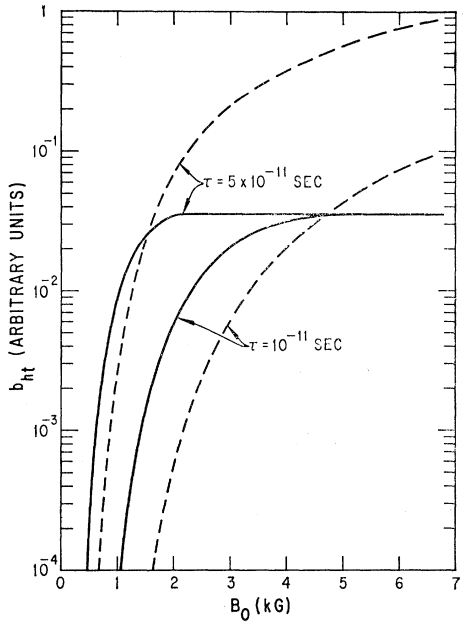

FIG. 4. Theoretical curves for b_{ht} as a function of B_0 for damped Alfvén wave propagation with $\mathbf{B}_0,\mathbf{k}\|2$ and the fundamental wave polarized $\|1$. The solid curves represent the magnitude of b_{ht1} and the dashed curves the magnitude of b_{ht3}. The curves were calculated for two values of $\tau(\tau_e=\tau_h=\tau)$ as indicated in the figure. Values for the effective masses are from Y. H. Kao, Phys. Rev. **129**, 1122 (1963).

and Table I for the special cases listed there. In this paper we have not tried to make quantitative comparison with theory for the magnetic-field dependence of the harmonic generation due to the uncertainties introduced by the geometrical effect. Even though two of the nonlinear coefficients, S_{222} and S_{311}, have been evaluated (Appendix C), we have not been able to satisfactorily compare the experimentally observed ratio of the harmonic signal to the fundamental signal with theory for several reasons. One is the geometrical effect mentioned above which may not be the same for the two signals. In addition, the magnitude of the harmonic is usually quite sensitive to the value used for τ, and knowledge of the value of the fundamental magnetic field at the surface of the sample is required. In Ref. 1 we estimated that the magnitude of the effect should be $\sim$10 times greater than that observed experimentally. The expressions used in that paper were not valid, however. If we use the results of the present paper and ignore the geometrical effect, an order-of-magnitude calculation for low values of $B_0(\mathbf{B}_0,\mathbf{k}\|3)$ leads to about the same result as we reported earlier. In view of the uncertainties in the calculation which we have mentioned, this sort of disagreement between theory and experiment is not unreasonably large.

In the subsections below, specific details of the damped Alfvén results for the three principal orientations are given.

$B_0,k\|2$

The harmonic curves shown in Fig. 3 were obtained when the fundamental field was polarized in the 1 direction. For the magnetic-field range covered, $|b_{ht1}| \gg |b_{ht3}|$. This configuration is relatively simple to treat theoretically since only one coefficient, S_{311}, is involved in the expressions for $b_{p1}{}^0$ and $b_{p3}{}^0$ given in Table I. We have used these expressions in Eq. (13) to calculate the relative magnitudes of b_{ht1} and b_{ht3} as is shown in Fig. 4. The difference in the harmonic curves for these two cases results from the fact that $b_{p3}{}^0 \propto B_0\tau b_{p1}{}^0$ when $\omega\tau\ll 1$. b_{ht1} would vanish completely if $\rho_{13}{}^0=0$ for $\mathbf{B}_0\|2$. When $\tau=10^{-11}$ sec, $b_{ht1}\gg b_{ht3}$ at low B_0. Although the theoretical curves cross at high B_0, this crossover was not observed experimentally. When the fundamental damped Alfvén wave is polarized in the 3 direction, the theoretical expressions for $b_{p1}{}^0$ and $b_{p3}{}^0$ are complicated by the fact that two coefficients, S_{113} and A_{313}, are involved. Experimentally, we found that the curve for b_{ht1} was very similar to the dashed curve in Fig. 3. The curve for b_{ht3} peaks at $\sim$4.5 kG at a value $\sim\times 2$ higher than the dashed curve in Fig. 3. This indicates that A_{313} is probably the dominant coefficient. If S_{113} were dominant, the same polarization observed for $\mathbf{b}_f\|1$ would have been seen.

$B_0,k\|3$

This orientation was discussed fairly extensively in Ref. 1. The components of the harmonic signal for the fundamental polarized in the 1 and 2 directions are shown in Fig. 5. According to Table I, the harmonic should be polarized in the 2 direction in both cases. The

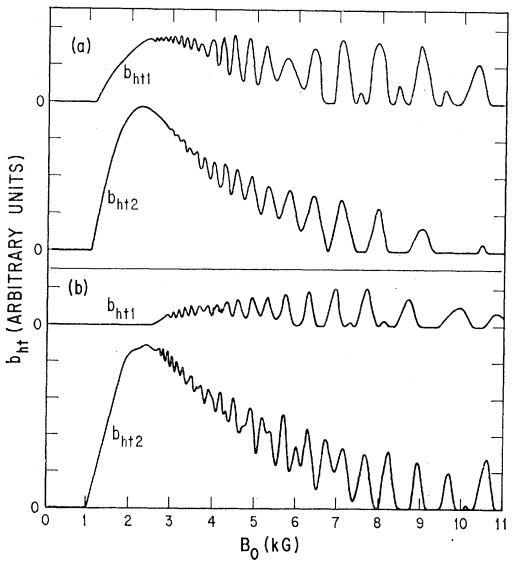

FIG. 5. Components of the 30-MHz harmonic signals as a function of B_0 for bismuth sample 75-4 with $\mathbf{B}_0,\mathbf{k}\|3$ at 1.2°K for the 15-MHz fundamental damped Alfvén signal polarized (a) $\|1$ and (b) $\|2$. The vertical scale is the same for all curves with the zeros displaced.

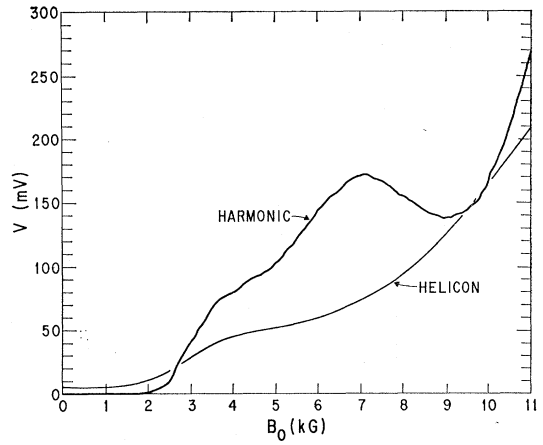

FIG. 6. Amplitude ($\times 10^5$) of the 30-MHz harmonic generated by a 15-MHz helicon wave (also shown) as a function of B_0 for Te-doped Bi sample 74-9A at 1.2°K with $\mathbf{B}_0,\mathbf{k}\|3$. The quantity $n-p$ in the sample was 2.5×10^{18} cm^{-3}.

experimental data are in reasonable agreement with theory. b_{ht1} is relatively large for $\mathbf{b}_f\|1$; however, this is probably a result of misorientation of the coils since the 1 and 2 axes are only 30° apart in the trigonal plane. It should be noted that the magnitude of the quantum oscillations are approximately the same in all cases. The theoretical curve for b_{ht2} is similar to the solid curves shown in Fig. 4 for $\mathbf{B}_0\|2$. The theoretical prediction for b_{ht1} is zero because $\rho_{12}{}^0=0$ when $\mathbf{B}_0\|3$.

$B_0,k\|1$

No effect is predicted for this orientation according to Table I. Experimentally this was verified except when $\mathbf{b}_f\|2$. In this case a relatively large signal was observed. The curve was similar in shape to the solid harmonic curve of Fig. 3 for $\mathbf{B}_0\|2;\mathbf{b}_f,\mathbf{b}_h\|1$, but it was scaled down by slightly more than a factor of 2. The observation of a signal for this orientation is probably a result of misorientation of the magnetic fields relative to the crystalline axes since $\mathbf{B}_0\|2;\mathbf{b}_f,\mathbf{b}_h\|1$ is only 30° away.

B. Helicon

Harmonic generation was observed for helicon propagation through Te-doped Bi samples for $\mathbf{k}$, $\mathbf{B}_0\|$ principal axes. It is difficult to compare results for the three orientations since the doping level and attenuation were quite different. Therefore, comments will be restricted to some qualitative statements. The effect observed when $\mathbf{B}_0$, $\mathbf{k}\|1$ or 2 seemed to be primarily due to quantum oscillations. No effect is predicted for $\mathbf{B}_0$, $\mathbf{k}\|1$, but the misorientation problem mentioned above in connection with the damped Alfvén data probably was responsible. No quantum oscillations were observed for $\mathbf{B}_0$, $\mathbf{k}\|3$ as can be seen in Fig. 6. The peaks in the harmonic curve result from Fabry-Perot resonances given by Eq. (13) similar to the resonance in the helicon transmission curve given by Eq. (12). We have not attempted to fit the harmonic curve using Eq. (13) and the values of $b_{p1}{}^0$ and $b_{p2}{}^0$ given in Table II.

V. CONCLUSIONS

The situation with regard to our present understanding of the observed effects is as follows:

(1) The occurrence of harmonics, and the dependence of the polarization of the harmonic on that of the fundamental which is summarized in Table I of Ref. 1, is completely consistent with the proposed mechanism, and our estimates indicate that this nonlinearity is dominant over all others. The nonlinearity arises because the dielectric constant of the meduim is a function of the magnetic field present, and particularly because it is sensitive to the magnetic-field component of the wave itself. This sensitivity occurs, in the case considered here, because of the anisotropy of the Fermi surface and its lack of reflection symmetry.

(2) The magnetic field dependence is understood qualitatively, and is influenced by geometrical effects related to the launching and detecting coils. The quantum oscillations are a manifestation of the Shubnikov–de Haas effect. A detailed analysis of these will not be possible until an experimentally confirmed theory of the Shubnikov–de Haas effect in bismuth is available. It is significant, however, that the mechanism which leads to the quantum oscillations is dominant for large $\mathbf{B}_0$.

ACKNOWLEDGMENTS

We wish to thank C. A. Collins for his able technical assistance, G. R. Cronin and D. Thompson for providing the bismuth crystals, and D. L. Carter, T. E. Hasty, and T. C. Penn for helpful conversations about various aspects of this work.

APPENDIX A: HARMONIC GENERATION IN A SLAB

We have treated the problem of harmonic generation in a slab by first applying the appropriate boundary conditions to Eq. (3) in order to find the magnetic field associated with the fundamental wave inside the slab. This solution for the fundamental wave is then used to

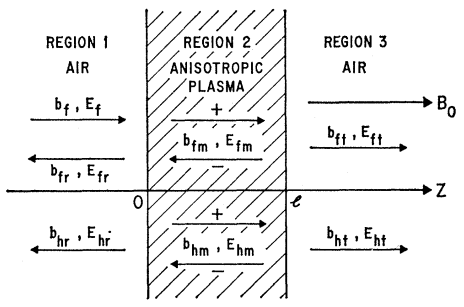

FIG. 7. Harmonic generation in an anisotropic plasma slab.

determine the source term in Eq. (4), and then the same boundary conditions are applied to the harmonic wave. This situation is illustrated in Fig. 7 for normal incidence with $\mathbf{B}_0$, $\mathbf{k}$, and $\mathbf{k}_s$ taken in the z direction. We carry out the calculation for the x component of $\mathbf{b}$ and the y component of $\mathbf{E}$, and suppress the subscripts x and y for simplicity. The fields associated with the fundamental wave in the three regions are given by the following:

Region 1

$$b_f = b_f{}^0 e^{i(\omega t-\omega z/c)},$$
$$E_f = -cb_f{}^0 e^{i(\omega t-\omega z/c)},$$
$$b_{fr} = b_{fr}{}^0 e^{i(\omega t+\omega z/c)},$$
$$E_{fr} = cb_{fr}{}^0 e^{i(\omega t+\omega z/c)};$$

Region 2

$$b_{fm} = b_{fm+}{}^0 e^{i(\omega t-kz)} + b_{fm-}{}^0 e^{i(\omega t+kz)},$$
$$E_{fm} = (-\omega b_{fm+}{}^0/k) e^{i(\omega t-kz)} + (\omega b_{fm-}{}^0/k) e^{i(\omega t+kz)};$$

Region 3

$$b_{ft} = b_{ft}{}^0 e^{i(\omega t-\omega z/c)},$$
$$E_{ft} = -cb_{ft}{}^0 e^{i(\omega t-\omega z/c)};$$

we have used $\nabla\times\mathbf{E}_f = -\partial\mathbf{b}_f/\partial t$ to relate the electric field components to the corresponding magnetic field components. The coefficients in the preceding equations can be evaluated in terms of $b_f{}^0$ by requiring that E_f and b_f be continuous at the two boundaries (assuming $\mu=\mu_0$ in all three regions). The magnetic field inside the plasma is given by

$$b_{fm} = \frac{2b_f{}^0[\cos k(l-z) + (ikc/\omega)\sin k(l-z)]e^{i\omega t}}{2\cos kl + i(\omega/kc + kc/\omega)\sin kl}. \quad \text{(A1)}$$

In the helicon and damped Alfvén wave experiments reported here, the condition $|kc/\omega| \gg 1$ holds. In addition, k is complex if we assume finite damping so that the denominator of Eq. (A1) can be simplified since the $\sin kl$ term does not vanish and always is much larger than the $\cos kl$ term in the region of interest. The contribution of the term $\cos k(l-z)$ is also negligible. Therefore,

$$b_{fm} \approx 2b_f{}^0 \sin k(l-z)\, e^{i\omega t}/\sin kl. \quad \text{(A2)}$$

In the analysis of our results we have also used the transmitted magnetic field just outside the second surface which is given by

$$b_{ft} \approx -2i\omega b_f{}^0 e^{i\omega(t-l/c)}/kc\,\sin kl, \quad \text{(A3)}$$

where again $|kc/\omega| \gg 1$. Equation (A3) appears in the test as Eq. (12).

Equation (A2) when substituted in Eq. (4) for the harmonic leads to a particular solution of this equation which is given by

$$b_p \approx -2b_p{}^0 \cos 2k(l-z)\, e^{i2\omega t}/\sin^2 kl, \quad \text{(A4)}$$

where the components of $\mathbf{b}_p{}^0$ are still defined by Eq. (9). Referring to Fig. 7, we have

Region 1

$$b_{hr} = b_{hr}{}^0 e^{i(2\omega t+2\omega z/c)},$$
$$E_{hr} = cb_{hr}{}^0 e^{i(2\omega t+2\omega z/c)};$$

Region 2

$$b_{hm} = [b_{hm+}{}^0 e^{-ik_s z} + b_{hm-}{}^0 e^{ik_s z} - 2b_p{}^0 \cos 2k(l-z)/\sin^2 kl]e^{i2\omega t},$$

$$E_{hm} = \left[\frac{-2\omega}{k_s} b_{hm+}{}^0 e^{-ik_s z} + \frac{2\omega}{k_s} b_{hm-}{}^0 e^{ik_s z} + \frac{2i\omega b_p{}^0 \sin 2k(l-z)}{k\sin^2 kl}\right]e^{i2\omega t};$$

Region 3

$$b_{ht} = b_{ht}{}^0 e^{i(2\omega t-2\omega z/c)},$$
$$E_{ht} = -cb_{ht}{}^0 e^{i(2\omega t-2\omega z/c)};$$

here we used $\nabla\times\mathbf{E}_h = -\partial\mathbf{b}_h/\partial t$. Requiring $\mathbf{b}_h$ and $\mathbf{E}_h$ to be continuous across the two boundaries and taking $|k_s c/2\omega| \gg 1$ leads to

$$b_{htx} = 8i\omega b_p{}^0 \frac{\sin[\tfrac{1}{2}(2k+k_s)l]\,\sin[\tfrac{1}{2}(2k-k_s)l]e^{i2\omega(t-l/c)}}{k_s c\,\sin k_s l\,\sin^2 kl}. \quad \text{(A5)}$$

Equation (A5) appears in the text as Eq. (13).

APPENDIX B: LIMITATIONS OF CRYSTAL SYMMETRY ON HARMONIC GENERATION IN AN EXTERNAL MAGNETIC FIELD

We consider here the case where nonlinear effects arise via the magnetic field component $\mathbf{b}$ of the wave. We ignore the influence of the electric field $\mathbf{E}$, an approximation which is valid for highly conducting materials.

The magnetoresistivity tensor $\boldsymbol{\varrho}$ is defined by the relations

$$\mathbf{E} = \boldsymbol{\varrho}(\mathbf{B}_0+\mathbf{b})\mathbf{J} \quad \text{(B1)}$$

and is considered a function of the static magnetic field $\mathbf{B}_0$ and of $\mathbf{b}$. Since $\mathbf{E}$ and $\mathbf{J}$ are polar or true vectors, $\boldsymbol{\varrho}(\mathbf{B}_0+\mathbf{b})$ is a second-rank polar tensor which is a function of the axial vectors $\mathbf{B}_0$ and $\mathbf{b}$. It is convenient to separate $\boldsymbol{\varrho}$ into symmetric and antisymmetric parts:

$$\rho_{ij}{}^s = \tfrac{1}{2}(\rho_{ij}+\rho_{ji}) = \rho_{ij}{}^s(\mathbf{B}) = \rho_{ji}{}^s(\mathbf{B}), \quad \text{(B2)}$$
$$\rho_{ij}{}^a = \tfrac{1}{2}(\rho_{ij}-\rho_{ji}) = \rho_{ij}{}^a(\mathbf{B}) = -\rho_{ji}{}^a(\mathbf{B}). \quad \text{(B3)}$$

The behavior of these tensors under time reversal, which reverses $\mathbf{B}$, is properly specified only by the Onsager relation

$$\rho_{ij}(\mathbf{B}) = \rho_{ji}(-\mathbf{B}), \quad \text{(B4)}$$

which gives

$$\rho_{ij}{}^s(\mathbf{B}) = \rho_{ij}{}^s(-\mathbf{B}), \quad \text{(B5)}$$
$$\rho_{ij}{}^a(\mathbf{B}) = -\rho_{ij}{}^a(-\mathbf{B}). \quad \text{(B6)}$$

TABLE III. Symmetry operations of $\bar{3}m$ point group.

1 or E	Identity
$\pm 3_2$ or $2C_3$	Rotation by $\pm\frac{2}{3}\pi$ about 3 axis
$3(2_\perp)$ or $3C_2$	Rotation by $\pm\pi$ about each 1 axis
$\bar{1}$ or i	Inversion
$\pm\bar{3}_2$ or $2S_6$	Rotation by $\pm\frac{2}{3}\pi$ about 3 axis followed by inversion
$3(\bar{2}_\perp)$ or $3\sigma_v$	Rotation by $\pm\pi$ about three 1 axes followed by inversion

Thus $\rho_{ij}{}^s$ is even, or invariant under time reversal, and $\rho_{ij}{}^a$ is odd, and changes sign under time reversal. This means that Eq. (B1) is *not* invariant under time reversal, a fact which has caused some confusion in the literature, as pointed out by Shtrikman and Thomas.[10] Following Birss,[11] we shall call tensors which are invariant under time reversal i tensors, and those which change sign under time reversal c tensors.

Noting that $b \ll B_0$, we expand the symmetric and antisymmetric parts of the magnetoresistivity tensor in Taylor's series:

$$\rho_{ij}{}^s(\mathbf{B}_0+\mathbf{b})=\rho_{ij}{}^s(\mathbf{B}_0)+S_{ijk}(\mathbf{B}_0)b_k+S_{ijkl}(\mathbf{B}_0)b_kb_l+\cdots, \quad \text{(B7)}$$
$$\rho_{ij}{}^a(\mathbf{B}_0+\mathbf{b})=\rho_{ij}{}^a(\mathbf{B}_0)+A_{ijk}(\mathbf{B}_0)b_k+A_{ijkl}(\mathbf{B}_0)b_kb_l+\cdots.$$

(Summation over repeated indices is implied.) Application of Eqs. (B5) and (B6) to Eq. (B7) yields the following relations:

$$\begin{aligned} &\rho_{ij}{}^s(-\mathbf{B}_0)=\rho_{ij}{}^s(\mathbf{B}_0), && \rho_{ij}{}^a(-\mathbf{B}_0)=-\rho_{ij}{}^a(\mathbf{B}_0), \\ &S_{ijk}(-\mathbf{B}_0)=-S_{ijk}(\mathbf{B}_0), && A_{ijk}(-\mathbf{B}_0)=A_{ijk}(\mathbf{B}_0), \\ &S_{ijkl}(-\mathbf{B}_0)=S_{ijkl}(\mathbf{B}_0), && A_{ijkl}(-\mathbf{B}_0)=-A_{ijkl}(\mathbf{B}_0). \end{aligned} \quad \text{(B8)}$$

Since $\mathbf{b}$ is an axial vector, it is apparent from Eq. (B7) that S_{ijk} and A_{ijk} are axial tensors, and S_{ijkl} and A_{ijkl} are polar tensors. Since from Eq. (B8), $\rho_{ij}{}^a$, S_{ijk}, and A_{ijkl} change sign under time reversal (reversal of $\mathbf{B}_0$) they are c tensors, and, similarly, $\rho_{ij}{}^s$, A_{ijk}, and S_{ijkl} are i tensors. If $\mathbf{B}_0=0$, the c tensors vanish, and the i tensors become the usual weak-field galvanomagnetic tensors.[12]

TABLE IV. Symmetry operations for point group $\bar{3}m$ in presence of magnetic field.

Direction of B_0	Symmetry operations[a]	Magnetic point group
General	$1, \bar{1}$	$\bar{1}$
Binary plane	$1, \bar{1}, \bar{2}_z{}^*, 2_z{}^*$	**2/m**
Binary axis (1)	$1, \bar{1}, 2_z, \bar{2}_z$	$2/m$
Bisectrix axis (2)	$1, \bar{1}, \bar{2}_z{}^*, 2_z{}^*$	**2/m**
Trigonal axis (3)	$1, \bar{1}, \pm 3_z, \pm\bar{3}_z, 3(\bar{2}_\perp{}^*), 3(2_\perp{}^*)$	$\bar{3}$**m**

[a] The asterisk indicates the time reversal operation.

[10] S. Shtrikman and H. Thomas, Solid State Commun. **3**, 147 (1965); **3**, civ (1965).
[11] R. R. Birss, *Symmetry and Magnetism* (North-Holland Publishing Co., Amsterdam, 1964).
[12] H. J. Juretschke, Acta Cryst. **8**, 716 (1955).

TABLE V. Excerpt from Table 7 of Ref. 11.

Magnetic field direction	Magnetic point group	i tensors: Polar even ($\rho_{ij}{}^s, S_{ijkl}$)	i tensors: Axial odd (A_{ijk})	c tensors: Polar even ($\rho_{ij}{}^a, A_{ijkl}$)	c tensors: Axial odd (S_{ijk})	Axes x	y	z
General	$\bar{1}$	A_m	A_n	A_m	A_n	1	2	3
Binary plane	**2/m**	B_m	B_n	C_m	C_n	2	3	1
$\mathbf{B}_0 \parallel 1$	$2/m$	B_m	B_n	B_m	B_n	2	3	1
$\mathbf{B}_0 \parallel 2$	**2/m**	B_m	B_n	C_m	C_n	2	3	1
$\mathbf{B}_0 \parallel 3$	$\bar{3}$**m**	L_m	L_n	M_m	M_n	2	−1	3

The number of independent nonvanishing tensor coefficients in Eq. (B7) is limited by the symmetry of the crystal, and the forms of the tensors for the $\bar{3}m$ point group characteristic of bismuth, for $\mathbf{B}_0=0$, are well known.[12] When an external field is applied, the only conventional symmetry operations of the crystal which are preserved are those which leave the direction of $\mathbf{B}_0$ in the crystal unchanged. If the additional operation of time reversal is allowed, conventional operations which reverse $\mathbf{B}_0$, combined with time reversal, are also symmetry operations. The inclusion of time reversal as a symmetry operation defines a new category of point groups called magnetic point groups, which have been thoroughly investigated and applied to magnetic materials.[11]

The symmetry operations defining the $\bar{3}m$ point group are listed in Table III. The symmetry operations, including time reversal, denoted by addition of an asterisk to the conventional symbol, are given for various directions of $\mathbf{B}_0$ in Table IV. (It is important, when determining the symmetry operations, to remember that $\mathbf{B}_0$ is an axial vector.) We see that, in each case, the group of symmetry operations can be identified with a magnetic point group. The value of making this identification lies in the fact that the allowed form of the galvanomagnetic tensors has been determined for each of the magnetic point groups. These tensors are listed in Ref. 11. Table V gives entries from Table 7 of Ref. 11 which are relevant to the present discussion. The entries in columns 3–6 refer in turn to Tables 4(a)–4(f) of Ref. 11. The nonvanishing components of the tensors

TABLE VI. Nonvanishing tensor coefficients up to third rank.

Magnetic field direction	$\rho_{ij}{}^s(\mathbf{B}_0)=\rho_{ji}{}^s(\mathbf{B}_0)$	$\rho_{ij}{}^a(\mathbf{B}_0)=-\rho_{ji}{}^a(\mathbf{B}_0)$	$S_{ijk}(\mathbf{B}_0)=S_{jik}(\mathbf{B}_0)$	$A_{ijk}(\mathbf{B}_0)=-A_{jik}(\mathbf{B}_0)$
Binary (1)	$\rho_{11}{}^s$	$\rho_{23}{}^a$	$S_{111}S_{122}S_{123}$	$A_{231}A_{122}A_{123}$
	$\rho_{22}{}^s$		$S_{221}S_{312}S_{313}$	$A_{312}A_{313}$
	$\rho_{33}{}^s$		S_{331}	
	$\rho_{23}{}^s$		S_{231}	
Bisectrix (2)	$\rho_{11}{}^s$	$\rho_{12}{}^a$	$S_{121}S_{112}S_{113}$	$A_{231}A_{122}A_{123}$
	$\rho_{22}{}^s$	$\rho_{13}{}^a$	$S_{311}S_{222}S_{223}$	$A_{312}A_{313}$
	$\rho_{33}{}^s$		$S_{332}S_{333}$	
	$\rho_{23}{}^s$		$S_{232}S_{233}$	
Trigonal (3)	$\rho_{11}{}^s=\rho_{22}{}^s$	$\rho_{12}{}^a$	$S_{121}=-S_{222}$	$A_{231}=A_{312}$
	$\rho_{33}{}^s$		$S_{311}=S_{232}$	A_{123}
			$S_{112}=-S_{222}$	
			$S_{113}=S_{223}$	
			S_{333}	

TABLE VII. Forms of tensors $\delta\rho_{ij}^0$ for $\mathbf{B}_0$, $\mathbf{k}$ along principal axes.

$\mathbf{B}_0,\mathbf{k}\|1$	
$\delta\rho_{22}^0=\delta\rho_{33}^0=\delta\rho_{23}^0=\delta\rho_{32}^0=0$, to first order in $\mathbf{b}^0$	
$\mathbf{B}_0,\mathbf{k}\|2$	
$\delta\rho_{11}^0=S_{113}(2)b_3^0$	$\delta\rho_{13}^0=S_{311}(2)b_1^0-A_{313}(2)b_3^0$
$\delta\rho_{33}^0=S_{333}(2)b_3^0$	$\delta\rho_{31}^0=S_{311}(2)b_1^0+A_{313}(2)b_3^0$
$\mathbf{B}_0,\mathbf{k}\|3$	
$\delta\rho_{11}^0=-S_{222}(3)b_2^0$	$\delta\rho_{12}^0=-S_{222}(3)b_1^0$
$\delta\rho_{22}^0=S_{222}(3)b_2^0$	$\delta\rho_{21}^0=-S_{222}(3)b_1^0$

are listed in Tables 4(a)–4(f) opposite the appropriate letter and subscript combination given in Table V. The proper assignment of axes is also found from Table V. The nonvanishing components of the second- and third-rank tensors obtained in this way for $\mathbf{B}_0$ along the three principal axes are given in Table VI. We have also derived them independently by application of the symmetry operations of the magnetic point groups. The connection to the theory of harmonic generation derived in the text is made by noting that the $\delta\rho_{ij}^0$ appearing in Eq. (9) are given, using Eq. (B7), by

$$\delta\rho_{ij}^0=\delta\rho_{ij}^{s0}+\delta\rho_{ij}^{a0}=\rho_{ij}^s(\mathbf{B}_0+\mathbf{b}^0)-\rho_{ij}^s(\mathbf{B}_0)+\rho_{ij}^a(\mathbf{B}_0+\mathbf{b}^0)-\rho_{ij}^a(\mathbf{B}_0)$$

or

$$\delta\rho_{ij}^0=S_{ijk}(\mathbf{B}_0)b_k^0+A_{ijk}(\mathbf{B}_0)b_k^0 \qquad \text{(B9)}$$

to first order in $\mathbf{b}^0$. For a general orientation of $\mathbf{k}$, Eq. (B9) will contain many terms. However, we are restricting our attention here to cases in which $\mathbf{B}_0$ and $\mathbf{k}$ are parallel to a principal axis of the crystal. In these cases, Eq. (B9) takes a simple form, and we have tabulated results for each of the principal axes in Table VII.

It is interesting to note that second harmonic generation of the type considered here cannot occur for $\mathbf{B}_0\|\mathbf{k}$ in any crystal when $\mathbf{k}$ is perpendicular to a reflection plane. To see this, we write

$$R_{ijk}(\mathbf{B}_0)=S_{ijk}(\mathbf{B}_0)+A_{ijk}(\mathbf{B}_0),$$

where $R_{ijk}(\mathbf{B}_0)$ is an axial tensor and $\mathbf{B}_0$ is an axial vector. If we reflect axis 1 in the 2-3 plane (reverse the 1 axis) noting that both $R_{ijk}(\mathbf{B}_0)$ and $\mathbf{B}_0$ change sign under such an improper rotation, we get $[\mathbf{B}_0=(B_1,B_2,B_3)]$

$$R_{ijk}(B_1,B_2,B_3)=-R_{ijk}'(B_1,-B_2,-B_3),$$

where $i, j, k\neq 1$, and the prime refers to the new coordinate system. If the 2-3 plane is a reflection plane, as is the case for Bi, we must have

$$R_{ijk}(B_1,B_2,B_3)=-R_{ijk}(B_1,-B_2,-B_3),$$

and, in particular,

$$R_{ijk}(B_1,0,0)=-R_{ijk}(B_1,0,0)=0 \quad (i,j,k\neq 1).$$

When $\mathbf{k}$ is parallel to axis 1, the dispersion relation contains only components of the type ρ_{ij}, $(i, j, k\neq 1)$, so that only third-rank tensor components of the type $R_{ijk}(\mathbf{B}_0)$, $(i, j, k\neq 1)$ produce harmonics, and they vanish for this case.

APPENDIX C: COMPUTATION OF NONLINEAR COEFFICIENTS FROM FERMI-SURFACE MODEL

In this section, we show how the nonlinear tensor coefficients $S_{ijk}(\mathbf{B}_0)$ and $A_{ijk}(\mathbf{B}_0)$ can be computed from the usual tilted-ellipsoid model of the Fermi surface of bismuth.

As a preliminary step, it is convenient, though not necessary, to write down expansions analogous to Eq. (B7) for the components of the *conductivity* tensor

$$\begin{aligned}\sigma_{ij}^s(\mathbf{B}_0+\mathbf{b})&=\sigma_{ij}^s(\mathbf{B}_0)+s_{ijk}(\mathbf{B}_0)b_k+\cdots,\\ \sigma_{ij}^a(\mathbf{B}_0+\mathbf{b})&=\sigma_{ij}^a(\mathbf{B}_0)+a_{ijk}(\mathbf{B}_0)b_k+\cdots.\end{aligned} \qquad \text{(C1)}$$

The nonvanishing coefficients in these expansions are those with the same indices as the coefficients appearing in Table VI. These coefficients are also required by symmetry to satisfy relations analogous to Eq. (B8). The coefficients $S_{ijk}(\mathbf{B}_0)$ and $A_{ijk}(\mathbf{B}_0)$ of Eq. (B7) can be expressed in terms of $s_{ijk}(\mathbf{B}_0)$ and $a_{ijk}(\mathbf{B}_0)$ of Eq. (C1) by means of the relations

$$\begin{aligned}&\sigma_{ij}(\mathbf{B}_0+\mathbf{b})\rho_{jk}(\mathbf{B}_0+\mathbf{b})=\delta_{ik},\\ &\sigma_{ij}^0\rho_{jk}^0=\delta_{ik} \quad [\sigma_{ij}^0=\sigma_{ij}(\mathbf{B}_0),\ \text{etc.}],\end{aligned} \qquad \text{(C2)}$$

which may be combined to yield the relation

$$S_{ijk}+A_{ijk}=-\rho_{ip}^0(s_{pqk}+a_{pqk})\rho_{qj}^0. \qquad \text{(C3)}$$

Separate expressions for S_{ijk} and A_{ijk} can be obtained from Eq. (C3) either by making use of Eqs. (B2) and (B3) or by using Eqs. (B8).

The coefficients $\sigma_{ij}^s(\mathbf{B}_0)$, $\sigma_{ij}^a(\mathbf{B}_0)$, $s_{ijk}(\mathbf{B}_0)$, and $a_{ijk}(\mathbf{B}_0)$ of Eq. (C1) are obtained in turn by writing down general expressions for $\sigma_{ij}(\mathbf{B}_0+\mathbf{b})$ using results given in Appendices I and II of Ref. 13. These results are derived classically assuming isotropic relaxation times and ignoring nonlocal effects. For a given component $\sigma_{ij}(\mathbf{B})$ the result is the sum of four contributions, one for each of the three electron ellipsoids (actually six hemiellipsoids) and one for the hole ellipsoid (two hemiellipsoids). If $\mathbf{B}_0$ and $\mathbf{b}$ are along principal crystallographic axes, and if terms of order b^2 are neglected, these contributions are of the form

$$\frac{\alpha+\beta b}{\gamma+\delta b}\approx\frac{\alpha}{\gamma}+\frac{1}{\gamma}\left(\beta-\frac{\alpha\delta}{\gamma}\right)b, \qquad \text{(C4)}$$

where α, β, γ, and δ depend on $\mathbf{B}_0$ and the mass-tensor components. These contributions are expanded as indicated on the right side of Eq. (C3) and summed over the four ellipsoids to give $\sigma_{ij}(\mathbf{B}_0)+[s_{ijk}(\mathbf{B}_0)+a_{ijk}(\mathbf{B}_0)]b_k$

[13] B. Lax *et al.*, Phys. Rev. **102**, 715 (1956); corrected expressions for $\mathbf{B}_0\|2$ are given by G. E. Smith, L. C. Hebel, and S. J. Buchsbaum, *ibid.* **129**, 154 (1963).

and broken up into symmetric and antisymmetric parts using Eq. (B8). Expressions for $\sigma_{ij}{}^{s}(\mathbf{B}_0)$, $\sigma_{ij}{}^{a}(\mathbf{B}_0)$, $s_{ijk}(\mathbf{B}_0)$, and $a_{ijk}(\mathbf{B}_0)$ can then be identified.

As an example, we carry out the procedure here for the simplest case, $\mathbf{B}_0$, $\mathbf{k}\|3$. Referring to Table VII, we see that, for $\mathbf{k}\|3$, the only nonlinear coefficient we need is $S_{222}(\mathbf{B}_0)$. Writing out Eq. (C3) for $S_{222}(3)$, using the nonvanishing coefficients from Table VI, we get

$$S_{222}(3)=-\rho_{22}{}^{0}{}^{2}s_{222}-\rho_{21}{}^{0}\rho_{12}{}^{0}s_{112}$$

or

$$S_{222}(3)=-[\rho_{11}{}^{0}{}^{2}(3)+\rho_{12}{}^{0}{}^{2}(3)]s_{222}(3)$$

$$=-\frac{s_{222}(3)}{\sigma_{11}{}^{0}{}^{2}(3)+\sigma_{12}{}^{0}{}^{2}(3)}=-\rho_{11}{}^{0}(3)\frac{s_{222}(3)}{\sigma_{11}{}^{0}(3)}. \quad \text{(C5)}$$

Expressions for $\sigma_{11}{}^{0}(3)$ and $\sigma_{12}{}^{0}(3)$ are given in Ref. 13. $s_{222}(3)$ is found by writing down, using the expressions in the Appendix of Ref. 13, the contributions of each ellipsoid to σ_{22}, assuming $b_1=0$, $\omega_c\tau\gg1$, and ignoring terms quadratic in b_2:

$$\sigma_{22}\text{ (ellipsoid 1)}=\frac{\sigma_0}{3}\frac{m_1m_3}{m_3b_3'^2+2m_4b_2'b_3'},$$

$$\sigma_{22}\text{ (ellipsoids 2 and 3)}=\frac{\sigma_0}{12}\frac{4m_3(m_1+3m_2)-12m_4^2}{4m_3b_3'^2-4m_4b_2'b_3'},$$

$$\sigma_{22}\text{ (holes)}=\sigma_{0h}\frac{M_1}{b_{3h}'^2},$$

where $\sigma_0=ne^2\tau_e/m_0$, $\sigma_{0h}=pe^2\tau_h/m_0$, $b_i'=eb_i\tau_e/m_0$, $b_{ih}'=-eb_i\tau_h/m_0$. Rewriting these contributions using Eq. (C4) we get

$$\sigma_{22}\text{ (ellipsoid 1)}=\frac{\sigma_0}{3}\frac{m_1}{b_3'^2}-\frac{2\sigma_0}{3}\frac{m_1m_4}{m_3b_3'^3}b_2',$$

$$\sigma_{22}\text{ (ellipsoids 2 and 3)}=\frac{\sigma_0}{12}\frac{m_3(m_1+3m_2)-3m_4^2}{m_3b_3'^2}$$

$$+\frac{\sigma_0}{12}\frac{m_3m_4(m_1+3m_2)-3m_4^3}{m_3^2b_3'^3}b_2',$$

$$\sigma_{22}\text{ (holes)}=\sigma_{0h}\frac{M_1}{b_{3h}'^2}.$$

Adding up these contributions, we get

$$\sigma_{22}(3)=\frac{\sigma_0}{b_3'^2}\frac{(m_1+m_2-m_4^2/m_3)}{2}+\frac{\sigma_{0h}}{b_{3h}'^2}M_1,$$

which agrees with Ref. 13, and

$$s_{222}(3)b_2=\frac{\sigma_0}{b_3'^3}\frac{b_2m_4}{m_3}(-\tfrac{1}{3}m_1+m_2-m_4^2/m_3).$$

For Bi, $m_1\ll m_2$, and if we let $m_2'=m_2-m_4^2/m_3$, we can write

$$\sigma_{11}(3)=\sigma_{22}(3)=\frac{m_0}{B_3^2}\left(\frac{nm_2'}{2\tau_e}+\frac{pM_1}{\tau_h}\right),\qquad \sigma_{12}(3)=\frac{e}{B_3}(n-p),$$

$$s_{222}(3)b_2=\frac{nm_0}{B_3{}^3\tau_e}\frac{m_4}{m_3}m_2'b_2.$$

From Eq. (C5) we now get

$$S_{222}(3)=-\rho_{11}{}^{0}(3)\frac{2m_4}{B_3m_3}\left(1+2\frac{pM_1\tau_e}{nm_2'\tau_h}\right)^{-1}, \quad \text{(C6)}$$

which is identical to the expression given earlier,[1] except that it is a factor of 2 larger. (The earlier expression was in error.) Assuming $p=n$, $\tau_e=\tau_h$, and using representative values of the mass parameters, we get

$$S_{222}(3)\approx-10\rho_{11}{}^{0}(3)B_3^{-1},$$
$$\rho_{11}{}^{0}(3)\approx2.3(B_3^2\tau/nm_0).$$

As a comparison, for the case, considered in the Introduction, of fast Alfvén waves propagating perpendicular to the field in an isotropic semimetal, the nonlinear coefficient is

$$S=2\rho_{\perp}{}^{0}B^{-1},\quad \rho_{\perp}{}^{0}=B^2\tau/nm^*,$$

where m^* is the effective mass, in units of m_0, of the two identical bands.

For $\mathbf{B}_0\|2$, the calculation of the nonlinear coefficients by this method becomes much more involved. The case $\mathbf{b}\|1$ also requires only one coefficient, $S_{311}(2)$. Assuming $n=p$, $\tau_e=\tau_h$, $m_1\ll m_2$, M_1 and $m_3\ll M_3$, our result is

$$S_{311}(2)\approx-3\frac{B_2\tau}{m_0n}\frac{m_4}{m_2M_3(1+3M_1/m_2)}. \quad \text{(C7)}$$